ELSEVIER

Journal of Structural Geology 29 (2007) 189–200

JOURNAL OF STRUCTURAL GEOLOGY

www.elsevier.com/locate/jsg

Numerical modeling of the motion of rigid ellipsoidal objects in slow viscous flows: A new approach

Dazhi Jiang*

Department of Earth Sciences, University of Western Ontario, London, Ontario, Canada N6A 5B7

Received 7 September 2006; received in revised form 12 September 2006; accepted 14 September 2006
Available online 16 November 2006

Abstract

A simple algorithm for modeling the rotation of rigid ellipsoidal objects in viscous flows based on Jeffery's (1922, Proceedings of the Royal Society of London A102, 161–179) theory is presented and is implemented in a fully graphic mathematics application Mathcad® (http://www.mathsoft.com). The orientation of ellipsoidal objects is specified in terms of polar coordinate angles that can be easily converted to the trend and plunge angles of the three principal axes rather than the Euler angles. With the Mathcad worksheets presented in the supplementary data associated with this paper, modeling the rotation paths of individual rigid objects, the development of inclusion trail geometry within synkinematic porphyroblasts, and the development of preferred orientation and shape fabrics for a population of rigid objects becomes as easy a task as using a spreadsheet. The shape and preferred orientation fabrics for a population of rigid objects can be presented in both a three-dimensional form and a two-dimensional form, allowing easy comparison between field data and model predictions. The modeler can customize the type and format of the output to best fit the purpose of the investigation and to facilitate the comparison of model predictions with geological observations. Application examples are presented for various types of modeling involving rigid objects.

Keywords: Rotation; Rigid clast; Fabric development; Preferred orientation; Jeffery's theory; Numerical modeling

1. Introduction

Jeffery's (1922) theory for the rotation of a rigid ellipsoidal object in a Newtonian fluid has been widely applied by geologists to the study of fabrics in rocks (e.g., Gay, 1966, 1968a,b; Ramsay, 1967, p. 225; Reed and Tryggvason, 1974; Hobbs et al., 1976, p. 285; Ghosh and Ramberg, 1976; Tullis, 1976; Harvey and Ferguson, 1978; Freeman, 1985; Passchier, 1987; Ježek et al., 1994, 1996; Arbaret et al,. 2000). The theory has been tested by many experiments (Taylor, 1923; Eirich and Mark, 1937; Trevelyan and Mason, 1951; Goldsmith and Mason, 1967; Ghosh and Ramberg, 1976; Ferguson, 1979; Arbaret et al., 2001), and Bretherton (1962) and Willis (1977) have extended the theory to include rigid objects of irregular, non-ellipsoidal shapes. There are many recent works in the geology literature on how the rotational behavior of rigid objects in a viscous flow may be affected by (1) the interface property between the matrix and the object (Ildefonse and Mancktelow, 1993; Mancktelow et al., 2002; Ceriani et al., 2003; Schmid and Podladchikov, 2004, 2005; Mandal et al., 2005b), (2) the boundary constraints where the rigid objects are large compared to the thickness of the hosting shear zone (Marques and Coelho, 2001), (3) the interaction between objects (Ildefonse et al., 1992a,b; Marques and Bose, 2004; Mandal et al., 2005b), and (4) the matrix anisotropy (Mandal et al., 2005a). However, whether applying Jeffery's theory directly to interpret geological fabrics or as a reference model against which to consider additional variables, it is always necessary to solve Jeffery's equations so that theoretical predictions are generated which can be tested by experiments and geological observations.

* Tel.: +1 519 661 3192; fax: +1 519 661 3198.
E-mail address: djiang3@uwo.ca

0191-8141/$ - see front matter © 2006 Elsevier Ltd. All rights reserved.
doi:10.1016/j.jsg.2006.09.010

For special cases, Jeffery's equations can be solved analytically. Jeffery (1922) himself provided the analytical solution for spheroids in simple shear flows. Gay (1966, 1968a) solved the equations for coaxial flows, and Ježek et al. (1996) found the analytical solutions for spheroids in all monoclinic flows. In the Supplement file, I present analytical solutions and summarize the rotation path patterns for spheroids in monoclinic flows using polar coordinate angles, rather than Euler angles, for specifying the orientation of objects. Beyond these special cases, Jeffery's equations must be solved numerically (Gierszewski and Chaffey, 1978; Hinch and Leal, 1979; Freeman, 1985; Ježek et al., 1994). In this respect, Ježek's (1994) programs are the most robust. They can be used to investigate the rotation path of an individual object as well as the evolution of the preferred orientation defined by a population of non-interacting rigid objects in any given flow field. The present paper develops a simple solution scheme for Jeffery's equations and implements it in a fully graphic mathematics application, Mathcad® (http://www.mathsoft.com). It advances the existing modeling of rigid objects in viscous flows in the following respects. First, in the present solution scheme, the orientation of the rigid object is specified by polar coordinate angles that are easily converted to the trend and plunge angles of the three principal axes of the object rather than the Euler angles used by Jeffery (1922), Bretherton (1962), Ježek (1994), and many others. Unlike the Euler angles, trend and plunge angles are measurable from geological observations and are easier to visualize. Second, the modeling predictions are presented in both a three-dimensional orientation/shape fabric form and a two-dimensional (sectional) orientation/shape fabric form. In many geological situations, the three-dimensional shape and orientation of a rigid object (such as a pebble) are not directly measurable unless the object is extractable; only the elliptical shape (axial ratios, R_f) and pitch angles (φ) of the ellipse's long axis on an exposed section are measurable (the R_f/φ type data of Ramsay, 1967; Dunnet, 1969). The present modeling allows direct comparison between model predictions and geological observations. Third, Mathcad® (http://www.mathsoft.com) is a fully graphic mathematics application. Modeling using the Mathcad worksheets provided with this paper is as user-friendly as using a spreadsheet. Finally, the solution scheme developed in this paper will be further extended in another paper (Jiang, in press) for numerical modeling of *deformable* ellipsoidal objects embedded in slow viscous flows based on the theory of Eshelby (1957, 1959).

2. Brief summary of Jeffery's theory

Before presenting the modeling scheme, it is necessary to briefly summarize Jeffery's (1922) theory which describes the motion of a single ellipsoidal rigid object embedded in a slow (inertial effects are therefore negligible) homogeneous flow of Newtonian fluid.

Let us denote the three semi-axes of the rigid ellipsoid a_1, a_2, and a_3. The three semi-axes can have any relative lengths, but for simplicity, we will adopt the following convention. For triaxial objects, we use a_1, a_2, and a_3 to represent, respectively, the long, intermediate, and the short semi-axes ($a_1 > a_2 > a_3$); for spheroidal objects (prolate and oblate ellipsoids) we use a_1 for the unique semi-axis and the other two semi-axes ($a_2 = a_3$, and mutually perpendicular) are arbitrarily defined on the plane normal to the a_1-axis. A right-handed coordinate system, $x'y'z'$, with x'-, y'-, and z'-axes parallel, respectively, to the a_1-, a_2-, and a_3-axes (Fig. 1), can be defined. This coordinate system rotates with the rigid object in a fixed external coordinate system, xyz, in which the flow of the matrix fluid is defined (Fig. 1). Let the unit vectors parallel to the x'-, y'-, and z'-axes be, respectively, $\mathbf{e}'_1$, $\mathbf{e}'_2$, and $\mathbf{e}'_3$ and those parallel to the x-, y-, and z-axes, respectively, $\mathbf{e}_1$, $\mathbf{e}_2$, and $\mathbf{e}_3$, and let the two coordinate systems have the same origin.

A position vector expressed by coordinates (x, y, z) in the xyz system is denoted $\mathbf{x}$. In the $x'y'z'$ system it is denoted $\mathbf{x}'$ with corresponding coordinates (x', y', z'). $\mathbf{x}$ and $\mathbf{x}'$ are related by:

$$\mathbf{x}' = \mathbf{Q}\mathbf{x} \tag{1a}$$

$$\mathbf{x} = \mathbf{Q}^{\mathrm{T}}\mathbf{x}' \tag{1b}$$

where $\mathbf{Q}$ is the coordinate transformation tensor ($\mathbf{Q}^{\mathrm{T}}$, its transpose) defined by:

$$\mathbf{e}'_i = \mathbf{Q}\mathbf{e}_i \tag{2a}$$

$$\mathbf{e}_i = \mathbf{Q}^{\mathrm{T}}\mathbf{e}'_i \tag{2b}$$

The homogeneous flow of the matrix is described in the xyz system by its Eulerian velocity gradient tensor $\mathbf{L}$ which can be

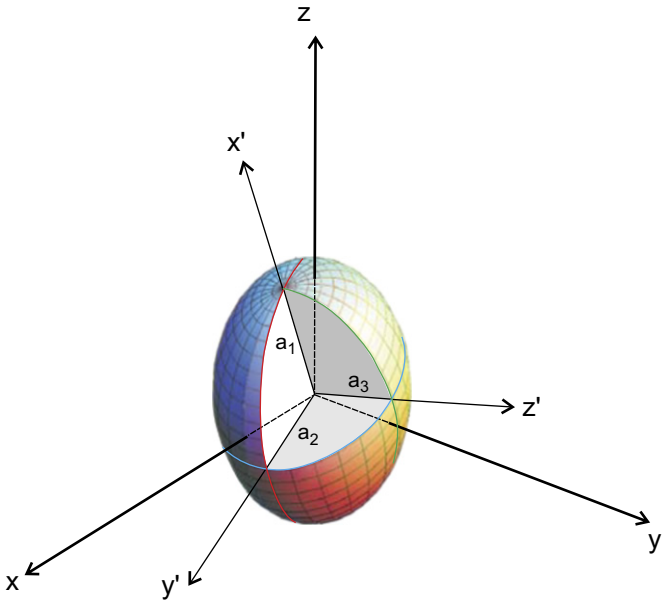

Fig. 1. External coordinate system xyz and the coordinate system parallel to the three principal axes of the rigid ellipsoid. a_1, a_2, and a_3 are the three semi-axes. The orientation of an ellipsoid in 3D space is defined by three polar coordinate angles. See text for details.

decomposed into a strain rate tensor **D** and a vorticity tensor **W** according to:

$$\mathbf{D}=\frac{1}{2}(\mathbf{L}+\mathbf{L}^{\mathrm{T}}),\quad \mathbf{W}=\frac{1}{2}(\mathbf{L}-\mathbf{L}^{\mathrm{T}}) \tag{3}$$

At any instant, the strain rate and the vorticity tensors expressed in the $x'y'z'$ system are, following the tensor transformation rule:

$$\mathbf{D}'=\mathbf{QDQ}^{\mathrm{T}},\quad \mathbf{W}'=\mathbf{QWQ}^{\mathrm{T}} \tag{4}$$

To define the shape of a rigid ellipsoidal object, Jeffery (1922) used its three shape factors, B_1, B_2, and B_3 defined as $B_1=(a_2^2-a_3^2)/(a_2^2+a_3^2)$, $B_2=(a_3^2-a_1^2)/(a_3^2+a_1^2)$, and $B_3=(a_1^2-a_2^2)/(a_1^2+a_2^2)$. Clearly, only two of the three shape factors are independent for it can be easily shown that $B_3=-(B_1+B_2)/(1+B_1B_2)$.

Jeffery (1922) shows that the rotation of the rigid ellipsoidal object is governed by an angular velocity determined by the matrix flow, the shape of the rigid object, and its instantaneous orientation in the flow. Expressed in the $x'y'z'$ coordinate system, this angular velocity is:

$$\boldsymbol{\omega}'=\begin{pmatrix}W'_{32}+B_1\cdot D'_{23}\\ W'_{13}+B_2\cdot D'_{13}\\ W'_{21}+B_3\cdot D'_{12}\end{pmatrix} \tag{5}$$

Following the vector transformation rule, the angular velocity (Eq. (5)), expressed in the xyz system, is:

$$\boldsymbol{\omega}=\mathbf{Q}^{\mathrm{T}}\boldsymbol{\omega}' \tag{6}$$

The rotation of the three principal axes of the rigid ellipsoid is described by the time rate of the three unit vectors parallel to their principal axes:

$$\frac{\mathrm{d}\mathbf{e}'_i}{\mathrm{d}t}=\boldsymbol{\omega}\times\mathbf{e}'_i=\boldsymbol{\Theta}\mathbf{e}'_i\ (i=1,\ 2,\ 3) \tag{7}$$

where $\boldsymbol{\Theta}$ is the tensor form of the angular velocity such that $\boldsymbol{\omega}\times\mathbf{p}\equiv\boldsymbol{\Theta}\mathbf{p}$ for any vector **p**, (e.g., Başar and Weichert, 2000, p. 30).

3. Specifying the orientation of a rigid ellipsoidal object

In this section, we express the above equations in terms of the orientation of the ellipsoidal object.

First, the orientation of a line can be represented by a unit vector parallel to it (e.g., Fisher et al., 1987). A unit vector, **u**, in 3D space xyz is completely defined by its two polar coordinate angles − the angle θ between x-axis and the projection of **u** on the xy-plane, and the angle ϕ between z-axis and **u** (Fig. 2a). The ranges for θ and ϕ are, respectively, $0\le\theta\le2\pi$ and $0\le\phi\le\pi$ (all angles are in radians unless otherwise indicated). In the geographic coordinate system (Fig. 2b), if $\phi\le\pi/2$ then θ is simply the plunge direction of **u** and $\pi/2-\phi$ is the plunge angle of **u**. If $\phi>\pi/2$ then $\theta\pm\pi$ is the plunge direction of **u** and $\phi-\pi/2$ is the plunge angle. By considering Fig. 2, the three components of **u** in the xyz system are related to its θ and ϕ by:

$$\mathbf{u}=\begin{pmatrix}u_1\\ u_2\\ u_3\end{pmatrix}=\begin{pmatrix}\cos\theta\sin\phi\\ \sin\theta\sin\phi\\ \cos\phi\end{pmatrix} \tag{8}$$

Second, the orientation of a triaxial ellipsoid is defined by the three unit vectors $\mathbf{e}'_1$, $\mathbf{e}'_2$, and $\mathbf{e}'_3$ parallel to its principal axes, each in turn being defined by its corresponding polar coordinate angles. However, because $\mathbf{e}'_1$, $\mathbf{e}'_2$, and $\mathbf{e}'_3$ are mutually perpendicular, only three polar angles are independent. In this paper, we use the triplet θ_1 and ϕ_1 (for the a_1-axis) plus θ_2 (for the a_2-axis) to define the orientation of a triaxial ellipsoidal object (Fig. 3a). For a spheroidal object, its orientation can be defined by the triplet made of the two polar angles of the unique axis (θ_1 and ϕ_1) plus an arbitrary θ_2. In the special case of a_1-axis being horizontal (i.e., $\phi_1=\pi/2$), the orientation of the ellipsoidal object can be defined by the triplet θ_1, ϕ_1 and ϕ_2 (Fig. 3b).

For $\mathbf{e}'_1$ (a_1-axis), we have:

$$\mathbf{e}'_1=\begin{pmatrix}\cos\theta_1\sin\phi_1\\ \sin\theta_1\sin\phi_1\\ \cos\phi_1\end{pmatrix} \tag{9}$$

By considering Fig. 4, it can be seen that the plunge angle of a_2-axis, ρ, is equal to the apparent dip of the a_2a_3-plane in the direction of θ_2. We therefore have $\rho=\tan^{-1}(\sin\kappa\tan\phi_1)$ which leads to $\phi_2=(\pi/2)+\tan^{-1}(\cos(\theta_1-\theta_2)\tan\phi_1)$ if $\phi_1\neq\pi/2$. As mentioned before, if $\phi_1=\pi/2$, ϕ_2 instead of θ_2 must be used as an independent variable to define the orientation of the object. In general, we therefore have, for $\mathbf{e}'_2$ (a_2-axis):

$$\mathbf{e}'_2=\begin{pmatrix}\cos\theta_2\sin\phi_2\\ \sin\theta_2\sin\phi_2\\ \cos\phi_2\end{pmatrix}=\begin{cases}\begin{pmatrix}-\sin\theta_1\sin\phi_2\\ \cos\theta_1\sin\phi_2\\ \cos\phi_2\end{pmatrix},\ \text{if } \phi_1=\dfrac{\pi}{2}\\[2ex] \begin{pmatrix}\cos\theta_2\cos[\tan^{-1}(\cos(\theta_1-\theta_2)\tan\phi_1)]\\ \sin\theta_2\cos[\tan^{-1}(\cos(\theta_1-\theta_2)\tan\phi_1)]\\ -\sin[\tan^{-1}(\cos(\theta_1-\theta_2)\tan\phi_1)]\end{pmatrix},\ \text{otherwise}\end{cases} \tag{10}$$

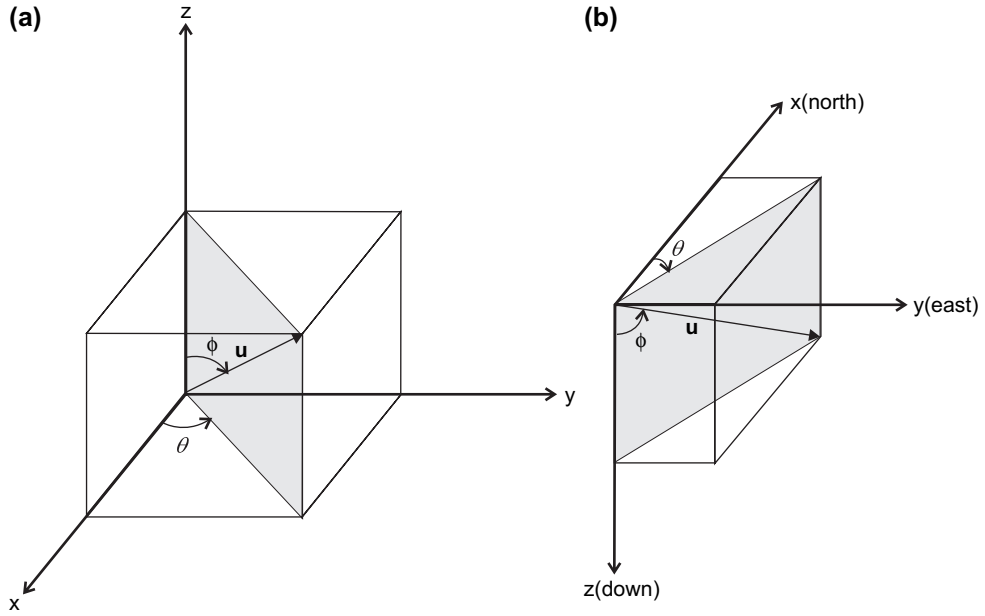

Fig. 2. (a) The orientation of a line in 3D space is represented by a unit vector, **u**. The two polar coordinate angles used in this paper to define the orientation of a line are: θ, the angle between the projection of **u** in xy-plane with the x-axis and ϕ the angle between **u** and the z-axis. (b) If xyz is a geographic coordinate system, then θ and ϕ are simply related to the trend and plunge of **u**. See text for details.

Finally, $\mathbf{e}'_3$ can be obtained by the cross product of $\mathbf{e}'_1$ and $\mathbf{e}'_2$:

$$\mathbf{e}'_3 = \mathbf{e}'_1 \times \mathbf{e}'_2 \tag{11}$$

The rotation tensor **Q** can now be expressed as:

$$\mathbf{Q} = \begin{pmatrix} \mathbf{e}_1'^{\mathrm{T}} \\ \mathbf{e}_2'^{\mathrm{T}} \\ \mathbf{e}_3'^{\mathrm{T}} \end{pmatrix} \tag{12}$$

By now we have expressed the terms on the right-hand side of Eq. (7) in terms of the orientation of the rigid object, its shape (B_1 and B_2), and the matrix flow. We now proceed with solving Eq. (7).

4. Rotation path of a single rigid object

Except for some special cases (Jeffery, 1922; Gay, 1966, 1968a; Ježek et al., 1996; Supplementary file), Eq. (7) must

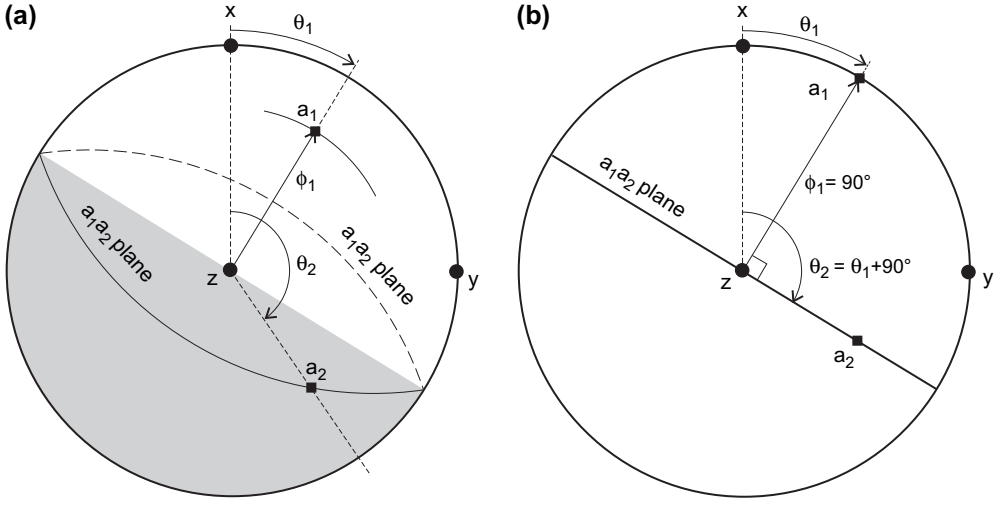

Fig. 3. Stereographic projection of the principal axes of a triaxial object demonstrating that the orientation of a triaxial ellipsoidal object can be uniquely defined by three polar coordinate angles: θ_1, ϕ_1 ($\neq \pi/2$) of the a_1-axis plus θ_2 for the a_2-axis (a). The diagram is for the case the down plunge direction is taken as the a_1-axis (plotting in the lower hemisphere, i.e. $\phi_1 < \pi/2$). Solid and dashed great circles are, respectively, lower and upper hemisphere projections of the a_2a_3-plane. If θ_2 lies in the shaded sector, a_1-axis and a_2-axis plot in the same hemisphere. Otherwise they plot in opposite hemisphere. (b) In the event $\phi_1 = \pi/2$, the three polar coordinate angles to define the orientation of the ellipsoid are θ_1, ϕ_1 and ϕ_2. The trend for the a_2-axis is taken as $\theta_2 = \theta_1 + \pi/2$, and ϕ_2 is the angle between coordinate z-axis and the a_2-axis direction associated with the θ_2. If $\phi_2 < \pi/2$, the a_2-axis lies in the lower hemisphere, otherwise it lies in the upper hemisphere. The directions of the a_1-, a_2-, and the a_3-axes are such that they form a right-handed coordinate system (Fig. 1). x, y, and z are geographic coordinate axes (Fig. 2b).

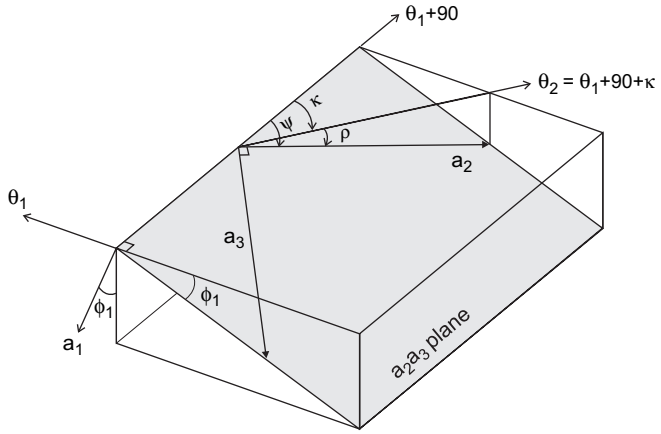

Fig. 4. The geometrical relationship between θ_2, the pitch (ψ) and plunge (ρ) of a_2-axis on the a_2a_3-plane (shaded) which is normal to the a_1-axis. κ: angle between trend of the a_2-axis and the strike of a_2a_3-plane. According to the definition of this paper $\phi_2 = \pi/2 - \rho$.

be solved numerically. To do so, we use the Runge–Kutta fourth-order method (e.g., Jeffrey, 1995, pp. 340–341) which for Eq. (7) leads to:

$$
\begin{aligned}
k_1 &= \delta t \boldsymbol{\Theta}(t_n)\mathbf{e}'_i(t_n)\\
k_2 &= \delta t \boldsymbol{\Theta}\left(t_n + \tfrac{\delta t}{2}\right)\left(\mathbf{e}'_i(t_n) + \tfrac{1}{2}\, k_1\right)\\
k_3 &= \delta t \boldsymbol{\Theta}\left(t_n + \tfrac{\delta t}{2}\right)\left(\mathbf{e}'_i(t_n) + \tfrac{1}{2}\, k_2\right)\\
k_4 &= \delta t \boldsymbol{\Theta}(t_n + \delta t)(\mathbf{e}'_i(t_n) + k_3)\\
\mathbf{e}'_i(t_{n+1}) &\approx \mathbf{e}'_i(t_n) + \frac{1}{6}(k_1 + 2k_2 + 2k_3 + k_4) \quad (i = 1,\ 2,\ 3)
\end{aligned}
\tag{13}
$$

where δt is a small time increment.

Being ultimately a function of the current orientation, $\mathbf{e}'_i(t_n)$, of the object once the shape of the object and the external flow are known, $\boldsymbol{\Theta}(t_n)$ in Eq. (13) can be calculated (Eqs. (5) and (6)) from the current orientation $\mathbf{e}'_i(t_n)$ of the object. To obtain $\boldsymbol{\Theta}(t_n + (\delta t/2))$ and $\boldsymbol{\Theta}(t_n + \delta t)$ for Eq. (13), we need to first obtain the object orientation at $t_n + (\delta t/2)$ and at $t_n + \delta t$. For this we use the Euler approximation $\mathbf{e}'_i(t_n + (\delta t/2)) \approx \mathbf{e}'_i(t_n) + (\delta t/2)\boldsymbol{\Theta}(t_n)\mathbf{e}'_i(t_n)$ and $\mathbf{e}'_i(t_n + \delta t) \approx \mathbf{e}'_i(t_n) + \delta t \boldsymbol{\Theta}(t_n)\mathbf{e}'_i(t_n)$.

Thus the right-hand side terms of Eq. (13) are all known from the current state. With Eq. (13), this leads to the new orientation $\mathbf{e}'_i(t_{n+1})$ of the object after a time increment δt. Continuing with this iterative procedure, one tracks the rotation path of the object from its initial orientation to its final orientation. The time increment δt controls the precision of the numerical calculation. The Runge–Kutta method is a very accurate method; the local error involved in the determination of $\mathbf{e}'_i(t_{n+1})$ from $\mathbf{e}'_i(t_n)$ is equivalent to the fifth order of δt (Jeffrey, 1995, p. 341). Therefore, an estimate of the error in the orientation of the object for each time step computation is then on the order of $|\boldsymbol{\omega}|(\delta t)^5$, where $|\boldsymbol{\omega}|$ is the magnitude of the instantaneous angular velocity. If we take an angular velocity of magnitude 1 Ma^{-1} ($\sim 3.17 \times 10^{-14}\ \mathrm{s}^{-1}$), using a $\delta t = 0.01$ Ma will yield an error on the order of 10^{-10} radians for each step of computation.

The *revolution* (Jiang and Williams, 2004) of the rigid object around its own principal axes, which is responsible for the inclusion trail curvature within a syn-kinematically grown porphyroblast, is described by the accumulated rotation (Ω) – the time integral of the angular velocity around the respective axis:

$$\Omega_i = \int_0^t \omega'_i \,\mathrm{d}t \quad (i = 1,\ 2,\ 3) \tag{14}$$

This can be approximated numerically according to:

$$\Omega_i \approx \sum_{m=1}^{n} \omega'_i(t_m) \cdot \delta t \quad (i = 1,\ 2,\ 3) \tag{15}$$

A Mathcad® worksheet (Worksheet 1, in Supplement file) is written based on the algorithm presented above. It can be used to model the rotation path of any ellipsoidal object. The output is in spreadsheet format that can be exported to any stereonet projection program for plotting the rotation paths.

5. Rotation of a population of non-interacting rigid objects

Jeffery's theory was developed for a single isolated ellipsoidal rigid object. For a system of many rigid inclusions in a viscous flow, if the inclusions are spaced far apart from one another so that they do not interact, Jeffery's theory would still be applicable. The work of Mandal et al. (2003) suggests that for pure shear flows if the spacing between adjacent objects is greater than twice the size of the object, they are practically non-interacting. Rotation of a large population of elongate rigid objects can result in two types of fabrics: a preferred orientation fabric (Ježek et al., 1994, 1996) defined by the alignment of the principal axes of the rigid objects and a shape fabric.

To model the development of these two types of fabrics, the solution scheme developed above for a single object must be extended. One must first define the initial state of all the rigid objects, i.e., the shape and orientation of each and every object. For a population of N rigid objects, this means N sets of (θ_1, ϕ_1, θ_2, B_1, B_2). Secondly, the numerical calculation must track the rotation of each and every object for a given flow to a given state of deformation.

5.1. Generation of the initial dataset and the evolution of the orientation fabric

In forward modeling of fabric development of a population of rigid objects, it is necessary to first generate a dataset of rigid objects that follow certain distributions. In the following, I first describe how to generate a set of lines following a given distribution in 3D space, and then extend the method to

generating a dataset for triaxial objects whose orientations and/or shapes follow certain distributions.

To generate a dataset of lines with uniform random distribution in 3D space, (Ramsay, 1967, pp. 163–164) and Sanderson and Meneilly (1981) use a brute force method by placing a uniform square grid at random over an equal-area stereonet and reading the trend and plunge of each and every grid points. While this method has been used by others (e.g., Ježek, 1994; Ježek et al., 1996), it is tedious, especially if one wants to have a large population of lines. It is not applicable if the distribution is not uniform. A general method for generating a set of randomly distributed lines is described below.

Considering the surface of a unit sphere (Fig. 5), the area element in the vicinity of a vector oriented at (θ, ϕ) is

$$dS = \sin\phi \cdot d\phi \cdot d\theta = -d(\cos\phi) \cdot d\theta \tag{16}$$

Uniform distribution in 3D of a population of vectors requires giving every area element of the same size identical probability for a line to intersect. This means that θ must be uniformly distributed in its entire range of [0, 2π], and cos(ϕ) must be uniformly distributed in its entire range of [−1, 1]. It is very simple to use a random number generator such as a spreadsheet to generate a population of random numbers following uniform distribution in the range [0, 2π] for θ, and another population of random numbers following the same distribution in the range [−1, 1]. Converting the latter population of numbers to the corresponding set of ϕ's using their inverse cosines, a set of (θ, ϕ) representing a uniformly distributing set of lines is generated. The above method also applies to any other type of distribution for the lines in 3D space.

Because each triaxial rigid object requires a triplet (θ_1, ϕ_1, θ_2) to define its orientation in 3D, after generating the population for the first two variables (the polar angles for the a_1-axis), we must find an associated population of θ_2's to complete the initial dataset for the orientations of the ellipsoidal objects. Considering Fig. 4, in order for a_2-axes to be uniformly distributed, their pitches (ψ, see Fig. 4) on the a_2a_3-plane must be uniformly distributed in its entire range [0, π]. The following relationship can be obtained by considering Fig. 4:

$$\kappa = \tan^{-1}(\cos\phi_1 \tan\psi) \tag{17a}$$

$$\theta_2 = \theta_1 + \frac{\pi}{2} + \kappa = \theta_1 + \frac{\pi}{2} + \tan^{-1}(\cos\phi_1 \tan\psi) \tag{17b}$$

Therefore, we can generate a population of random numbers between 0 and π using a spreadsheet for ψ and then calculate the corresponding set of θ_2 using Eq. (17b).

Fig. 6a–c presents lower hemisphere equal-area projections of the orientations of a population of 300 triaxial objects generated according to the method described above.

One may also make the variability of B_1 and B_2 (or equivalently a_1/a_2 and a_1/a_3) follow certain distribution. Once the initial dataset is complete, modeling the evolution of the orientation fabric defined by the axes can be readily carried out using an algorithm slightly modified from the one for single object (Worksheet 2, Supplement file).

5.2. Shape fabric of rigid objects as observed on a section of arbitrary orientation

As noted by some authors (e.g., Giorgis and Tikoff, 2004), it is generally hard to obtain directly the 3D data of ellipsoidal clasts. An ellipsoidal object exposes on a 2D section as an ellipse. In many cases what one can directly measure in the field are the aspect ratios (R_f) of the sectional ellipses and the pitch angles (φ) of the long axes of the ellipses – the well-known R_f/φ data (Ramsay, 1967, Chapter 5; Dunnet, 1969; Lisle, 1985). It is therefore desirable to generate similar modeling output that can be directly compared with field observations. This is developed in the following.

The ellipsoidal surface of the object in the $x'y'z'$ system can be expressed as:

$$\frac{x'^2}{a_1^2} + \frac{y'^2}{a_2^2} + \frac{z'^2}{a_3^2} = 1, \quad \text{or} \quad (x' \;\; y' \;\; z') \begin{pmatrix} \frac{1}{a_1^2} & 0 & 0 \\ 0 & \frac{1}{a_2^2} & 0 \\ 0 & 0 & \frac{1}{a_3^2} \end{pmatrix} \begin{pmatrix} x' \\ y' \\ z' \end{pmatrix}$$

$$= (x' \;\; y' \;\; z')\mathbf{G}' \begin{pmatrix} x' \\ y' \\ z' \end{pmatrix} = 1 \tag{18}$$

Since we are only concerned with the shape, rather than the absolute size, of the ellipsoid, the a_3-axis can be set to unity and $\mathbf{G}'$ in Eq. (18) can be expressed in terms of B_1 and B_2 of the ellipsoid:

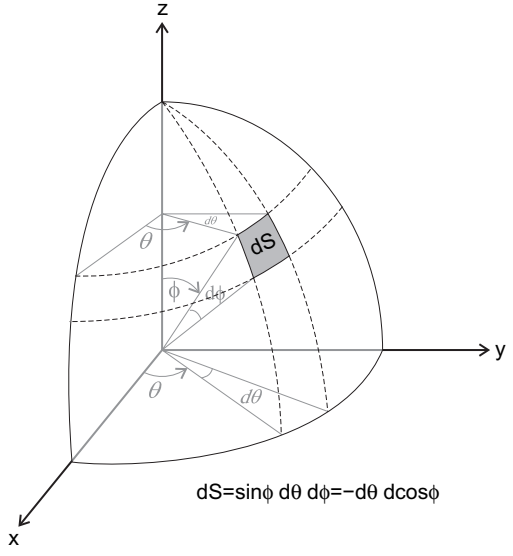

Fig. 5. An infinitesimal area element, dS, on the surface of a unit sphere is expressed in terms of an infinitesimal increment in θ and an infinitesimal increment in cos(ϕ). For a population of lines following certain distribution (such as uniform) over the sphere, both θ and cos(ϕ) must follow that distribution. See text for details.

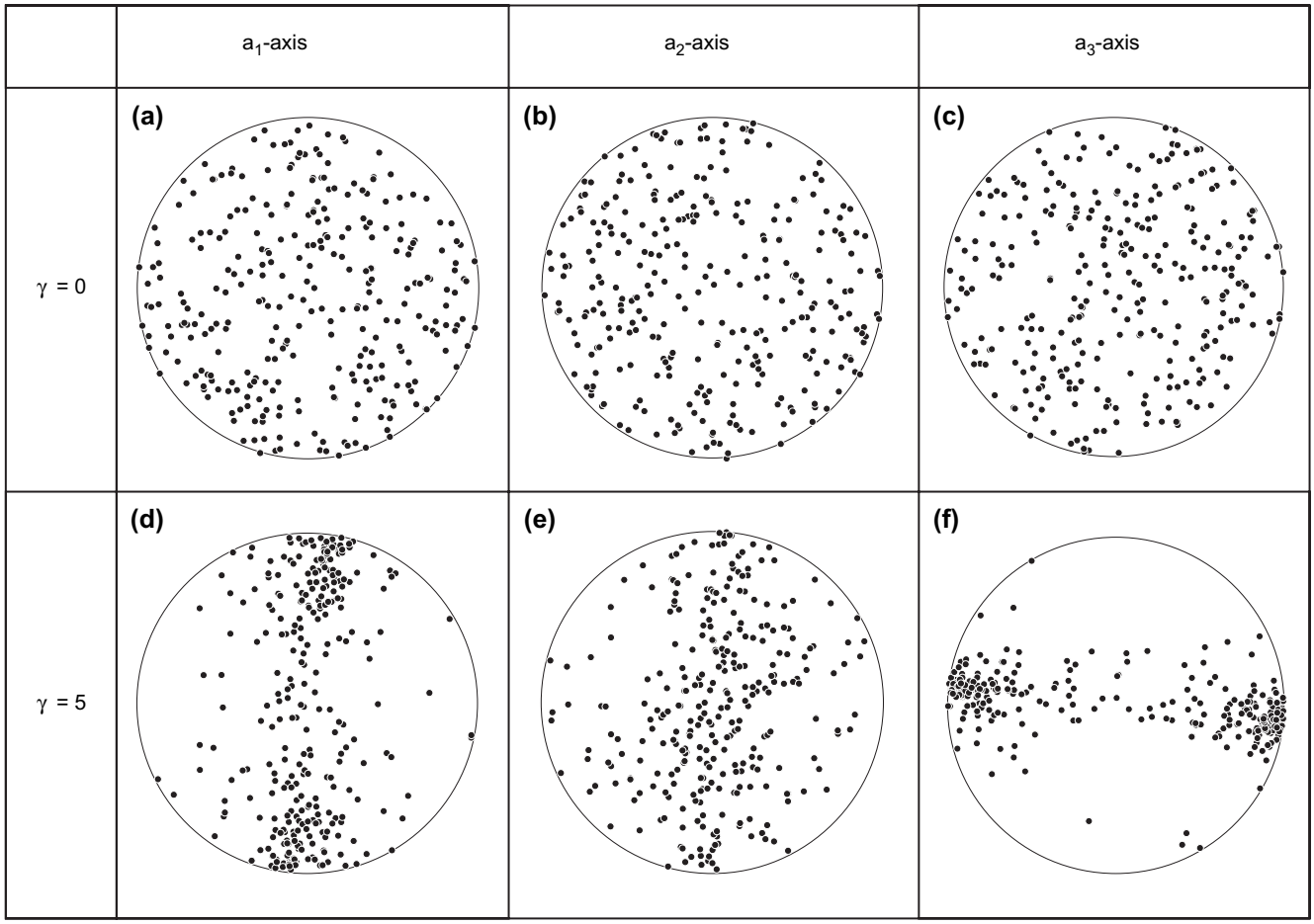

Fig. 6. (a–c) Lower hemisphere equal-area plot of the three principal axes of 300 triaxial objects (all 5:3:1) with uniform distribution (data generated using the method described in the text). (d–f) After a shear strain of 5 in simple shear, the orientation fabric defined by the three axes, respectively. For orientation of the flow, see Fig. 10d.

$$\mathbf{G}' = \begin{pmatrix} \frac{1+B_2}{1-B_2} & 0 & 0 \\ 0 & \frac{1-B_1}{1+B_1} & 0 \\ 0 & 0 & 1 \end{pmatrix} \tag{19}$$

In the external coordinate *xyz*, the ellipsoid tensor $\mathbf{G}'$ is expressed, following a tensor transformation, as:

$$\mathbf{G} = \mathbf{Q}^{\mathrm{T}}\mathbf{G}'\mathbf{Q} \tag{20}$$

The eigenvalues of $\mathbf{G}$ are the squares of the inverse of the three principal axes of the ellipsoid and the corresponding eigenvectors their directions.

Consider a geological plane (M) striking at α and dipping at β which cuts across the ellipsoid (Fig. 7). To explain how R_f and φ for the ellipse on M are calculated from $\mathbf{G}$, consider a right-handed coordinate system, $\chi\eta\xi$, with χ-axis parallel to the strike of M, η-axis parallel to the dipline of M, and ξ-axis normal to M and pointing down (Fig. 7). By considering Fig. 7, in the *xyz* system, the three unit vectors parallel to the χ-, η-, and ξ-axis are evidently:

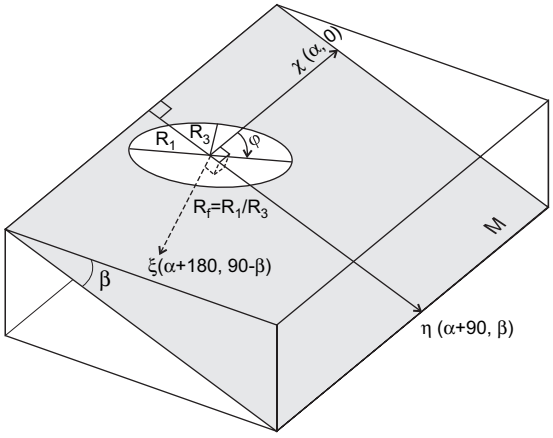

Fig. 7. On a geological section (M) an ellipsoidal object exposes as an ellipse. The axial ratio (R_f) and the pitch (φ) of the long axis can be measured. $\chi\eta\xi$ is the coordinate system for calculating R_f and φ once the dip of M is given and the ellipsoidal tensor is known. See text for details.

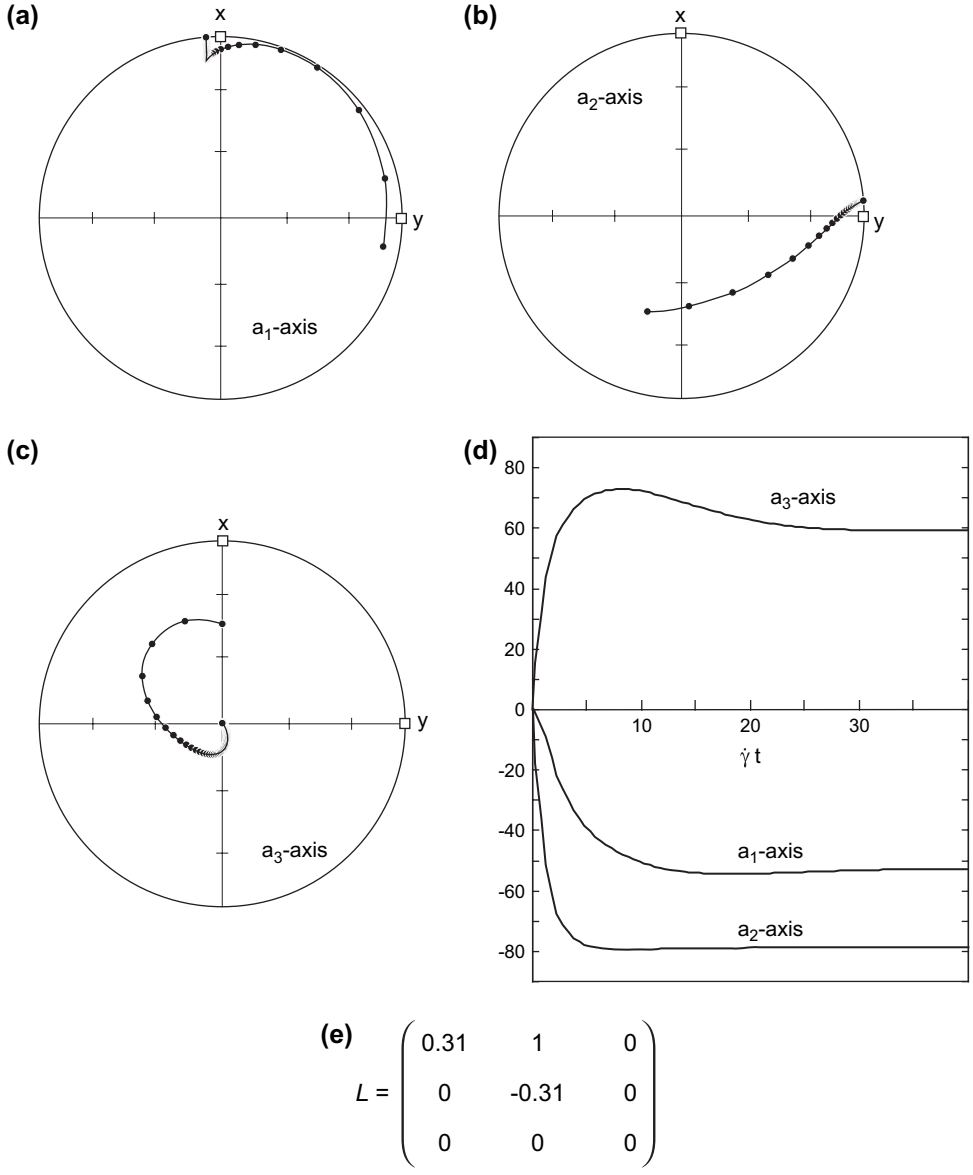

Fig. 8. Rotation paths (a–c) and revolutions (d) for the principal axes of a triaxial ellipsoid (5:3:1) in a plane-strain flow (e). Initial orientation of the object: a_1-axis: 10°, 100°, a_2-axis 45°, 360°, and a_3-axis: 44°, 200°. See text for details.

$$\boldsymbol{\chi} = \begin{pmatrix} \cos\alpha \\ \sin\alpha \\ 0 \end{pmatrix}, \quad \boldsymbol{\eta} = \begin{pmatrix} -\sin\alpha\cos\beta \\ \cos\alpha\cos\beta \\ \sin\beta \end{pmatrix}, \quad \boldsymbol{\xi} = \begin{pmatrix} \sin\alpha\sin\beta \\ -\cos\alpha\sin\beta \\ \cos\beta \end{pmatrix} \tag{21}$$

which yields the following tensor that transforms *xyz* coordinates to $\chi\eta\xi$ coordinates:

$$\mathbf{Q}_1 = \begin{pmatrix} \cos\alpha & \sin\alpha & 0 \\ -\sin\alpha\cos\beta & \cos\alpha\cos\beta & \sin\beta \\ \sin\alpha\sin\beta & -\cos\alpha\sin\beta & \cos\beta \end{pmatrix} \tag{22}$$

The ellipsoid tensor expressed in the $\chi\eta\xi$ coordinate system is then:

$$\mathbf{G}_{\chi\eta\xi} = \mathbf{Q}_1\mathbf{G}\mathbf{Q}_1^{\mathrm{T}} = \mathbf{Q}_1\mathbf{Q}^{\mathrm{T}}\mathbf{G}'\mathbf{Q}\mathbf{Q}_1^{\mathrm{T}} \tag{23}$$

The shape and orientation of the ellipse as observed on plane *M* are described by the following sub-matrix of $\mathbf{G}_{\chi\eta\xi}$:

$$\mathbf{G}_{\mathrm{sub}} = \begin{pmatrix} (\mathbf{G}_{\chi\eta\xi})_{11} & (\mathbf{G}_{\chi\eta\xi})_{12} \\ (\mathbf{G}_{\chi\eta\xi})_{21} & (\mathbf{G}_{\chi\eta\xi})_{22} \end{pmatrix} \tag{24}$$

The aspect ratio R_{f}, and pitch φ of the long axis of the ellipse as observed on plane *M* can be obtained from the eigenvalues and eigenvectors of $\mathbf{G}_{\mathrm{sub}}$.

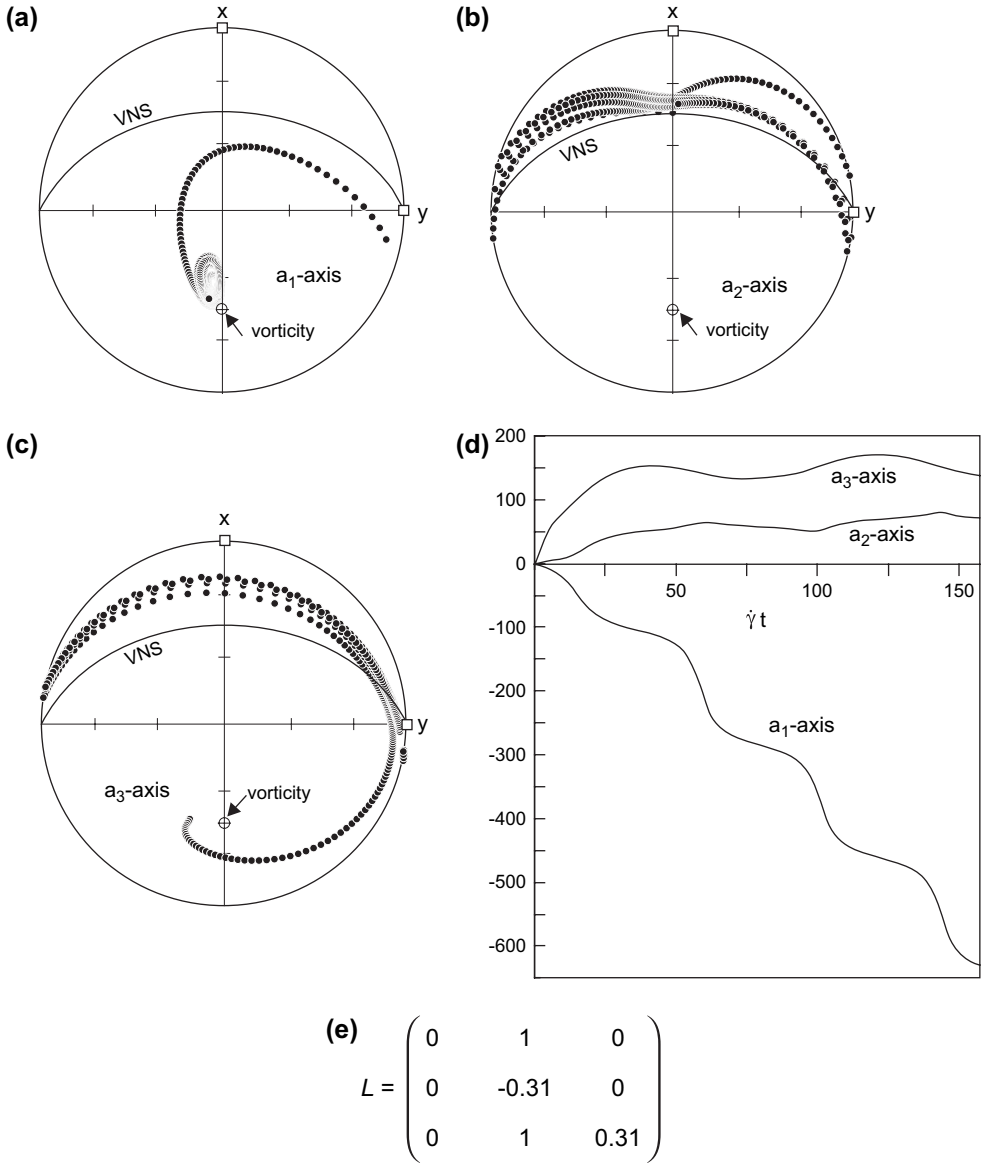

Fig. 9. Rotation paths (a–c) and revolutions (d) for the principal axes of a triaxial ellipsoid (5:3:1) in a triclinic flow (e). Initial orientation of the object: a_1-axis: 10°, 100°, a_2-axis 45°, 360°, and a_3-axis: 44°, 200°. VNS: vorticity-normal section. See text for details.

6. Applications

The Mathcad® worksheets (Supplement) of this paper can be used for investigating (1) the motion of a single rigid object in any given 3D viscous flows, (2) inclusion trail development in syn-kinematically grown porphyroblasts, and (3) development of preferred orientation and shape fabric for a population of rigid objects of given initial orientation and shape distribution. These applications are described in more detail in the following.

6.1. Rotation path and revolution of individual rigid objects

The motion of a triaxial rigid object of any shape can be approximated by that of an ellipsoidal object (Bretherton, 1962; Willis, 1977; Arbaret et al., 2001). In the limit, this includes material lines and planes. The Mathcad® Worksheet 1 (Supplement) can be applied to investigate the rotational behavior of a large variety of fabric elements. Jiang and Williams (2004) applied Worksheet 1 to investigate the rotation path of some triaxial and prolate rigid objects and the development of inclusion trails in syn-kinematically grown rigid porphyroblasts assuming that the shape of the porphyroblasts does not change. They demonstrated that the rotational behavior of elongated rigid objects is extremely complex even in simple flow regimes. A small difference in the initial orientation and/or shape of the object can result in drastically different final inclusion trail geometries. I present here two more examples to show the application of Worksheet 1 for modeling the rotation of individual rigid objects.

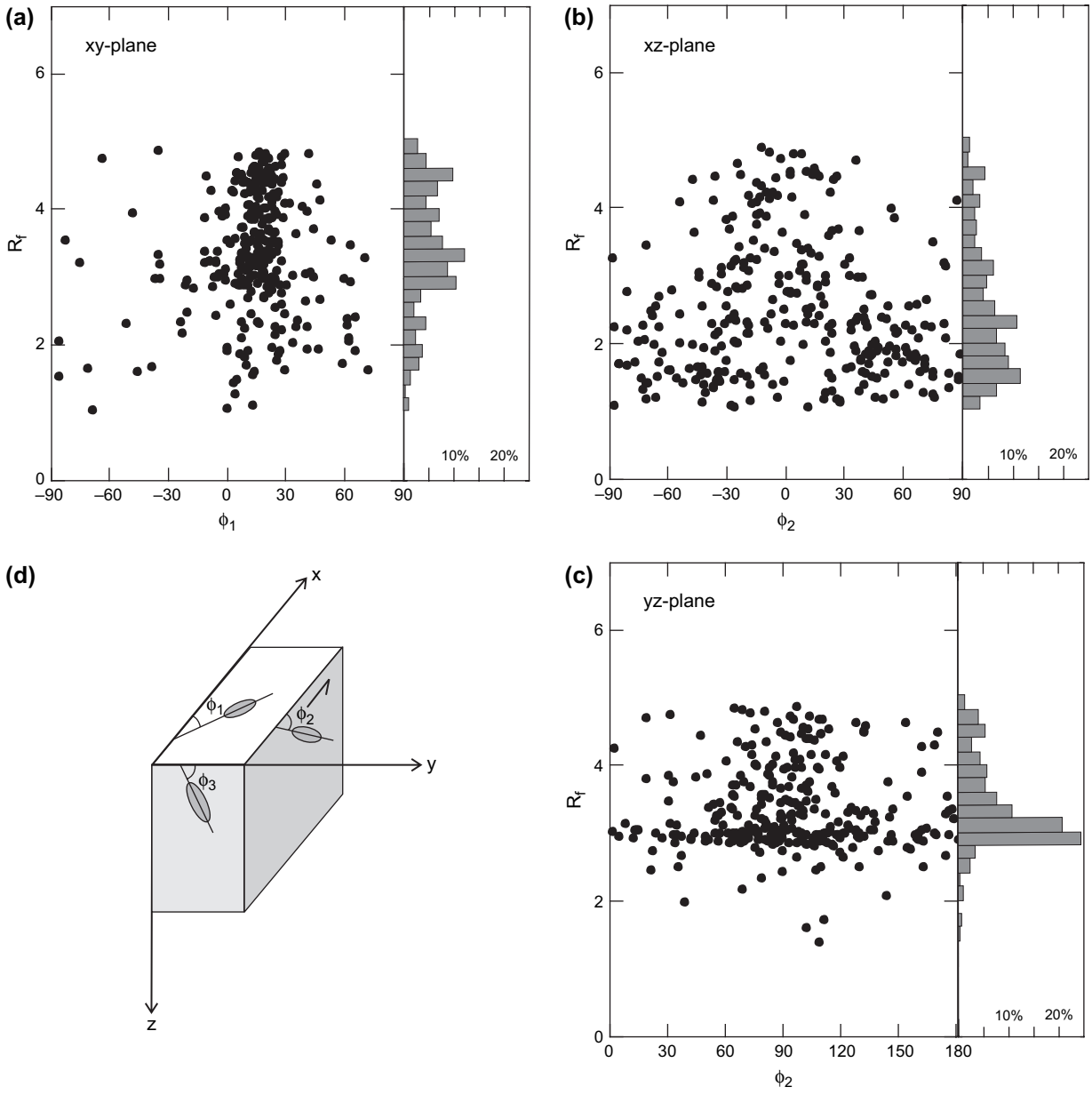

Fig. 10. R_f/φ plots (a–c) on three sections (orientation shown in (d)) at a shear strain of 5 under simple shear for a population of 300 triaxial objects (all 5:3:1) that are uniformly oriented initially (Fig. 5 a–c). The histogram associated with each section shows the 2D shape distribution of the ellipses. Data of this nature can be obtained for a plane of any orientation.

To apply the modeling, first provide the input variables in the "Input variables" part of the worksheet. The input variables include the flow velocity gradient tensor, **L**, (Fig. 8e), the shape factors of the object, the initial orientation of the object, and the incremental time size (δt). There are two additional variables, *mm* and *STEPS* in the worksheet. The variable *mm* specifies the number of steps of computation between output sets. In other words, in the output data, the time duration between successive states of the object is *mm* δt. The variable *STEPS* specifies the total number of steps of computation. The total actual time duration of deformation is therefore *STEPS* δt.

Fig. 8a–c presents the rotation paths for the three principal axes of a triaxial ellipsoid (5:3:1) with initial orientations: a_1-axis: 10°, 100°, a_2-axis 45°, 360°, and a_3-axis: 44°, 200° in a plane-strain flow (Fig. 8e). Fig. 8d is the revolution around each axis. All three axes reach stable orientations in this case. Fig. 9a–c presents the rotation paths for the three axes of a triaxial ellipsoid of the same shape and initial orientations as for Fig. 8 in a triclinic flow (Fig. 9e). Fig. 9d is the revolution around each axis. No axes reach a stable orientation although a_1-axis ends up very close to the vorticity vector at high strain.

6.2. Development of preferred orientation fabric and shape fabric for a population of rigid objects

To model the rotation of a population of rigid objects, Worksheet 2 (Supplement) is used. In addition to the flow

velocity gradient tensor, **L**, the time increment, δt, and the total steps of computation, the input variables include the dataset for the initial orientations and shapes of all the rigid objects and the number of objects. The initial orientations and shapes of objects are generated through Excel using the method described above and inserted into the worksheet. If the R_f/φ data on a plane is required, one must provide the strike and dip of the plane. The final output will include the trend and plunge angles of the principal axes of each and every object as well as the R_f/φ data on the 2D section.

Figs. 6 and 10 present results of an application of this program. For a group of 300 triaxial objects of the same shape (5:3:1) initially having uniform random distribution (Fig. 6a–c), in a simple shear deformation, at the state of shear strain 5, a preferred orientation is clearly defined (Fig. 6d–f). Fig. 10a–c presents the R_f/φ results for three sections (Fig. 10d) and the 2D clast shape distributions (histogram associated with each R_f/φ) as observed on the three sections.

6.3. Discussion: the use of rigid clast data to constrain natural deformation kinematic conditions

By numerical forward modeling approaches, field observations can be used to constrain natural deformation conditions. Lin et al. (1998) and Lin and Jiang (2001) use the lineation and foliation data from shear zones to constrain the boundary movement conditions of the zones. The modeling worksheets presented in the supplementary data associated with this paper will be useful for using shape and preferred orientation data of rigid clasts to constrain the deformation kinematics. Since in general only 2D data in the form of R_f/φ are obtainable from field measurement or from measurement on rock slabs in the laboratory, one way to represent these data is to best fit the 2D data on each section into a fabric ellipse using the method of Robin (1977) designed for strain analysis and then use the fabric ellipses from three or more sections to derive a 3D fabric ellipsoid using the method of Robin (2002) and Launeau and Robin (2005). Similarly, Worksheet 2 (Supplement) can readily predict the R_f/φ data on any given sections which can be used to derive the 3D fabric ellipsoid at any stage of deformation for given boundary conditions. The fabric ellipsoid determined from field data can then be compared with the model-produced fabric ellipsoid to test the soundness of the given deformation conditions.

7. Concluding remarks

The algorithm presented in this paper and its implementation in the fully graphic mathematics application (Mathcad®) make modeling based on Jeffery's theory much simpler than using command-line programs. The Mathcad worksheets allow the modeling of all aspects related to the motion of rigid objects, including (1) the rotation path of a single rigid object, (2) the development of inclusion trail geometry in synkinematic rigid porphyroblasts, and (3) the development of preferred orientation and shape fabrics for a population of rigid objects, to be performed in a unified modeling environment. The shape and preferred orientation fabrics for a population of rigid objects can be presented in both a 3D form and a 2D form, allowing easy comparison between field data and model predictions. The modeler can interact fully with the computation to customize the modeling so that the type and format of the output data best fit the purpose of the investigation.

Acknowledgements

I thank J. Ježek and K.F. Mulchrone for suggesting the use of a better numerical approximation than the initial Euler method. This has led to the current Runge–Kutta method used in this paper as well as an accompanying paper on the motion of deformable clasts. Support from NSERC discovery grant and the University of Western Ontario Academic Development Funds is acknowledged.

Appendix A. Supplementary data

Supplementary data associated with this article can be found, in the online version, at doi:10.1016/j.jsg.2006.09.010.

References

Arbaret, L., Fernandez, A., Ježek, J., Ildefonse, B., Launeau, P., Diot, H., 2000. Analogue and numerical modelling of shape fabrics: application to strain and flow determination in magmas. Transactions of the Royal Society of Edinburgh. Earth Sciences 91, 97–109.

Arbaret, L., Mancktelow, N.S., Burg, J.P., 2001. Effect of shape and orientation on rigid particle rotation and matrix deformation in simple shear flow. Journal of Structural Geology 23, 113–125.

Başar, Y., Weichert, D., 2000. Nonlinear Continuum Mechanics of Solids: Fundamental Mathematical and Physical Concepts. Springer, Berlin.

Bretherton, F.P., 1962. The motion of rigid particles in shear flow at low Reynolds number. Journal of Fluid Mechanics 14, 284–301.

Ceriani, S., Mancktelow, N.S., Pennacchioni, G., 2003. Analogue modelling of the influence of shape and particle/matrix interface lubrication on the rotational behaviour of rigid particles in simple shear. Journal of Structural Geology 25, 2005–2021.

Dunnet, D., 1969. A technique of finite strain analysis using elliptical particles. Tectonophysics 7, 117–136.

Eirich, F., Mark, H., 1937. Ueber Lösungsmittelbindung durch Immobilisierung. Papierfabrikant 27, 251–258.

Eshelby, J.D., 1957. The determination of the elastic field of an ellipsoidal inclusion, and related problems. Proceedings of the Royal society of London, A 241, 376–396.

Eshelby, J.D., 1959. The elastic field outside an ellipsoidal inclusion. Proceedings of the Royal society of London, A 252, 561–569.

Ferguson, 1979. Rotations of elongate rigid particles in slow non-Newtonian flows. Tectonophysics 60, 247–262.

Fisher, N.I., Lewis, T., Embleton, B.J.J., 1987. Statistical Analysis of Spherical Data. Cambridge University Press, Cambridge.

Freeman, B., 1985. The motion of rigid ellipsoidal particles in slow flows. Tectonophysics 113, 163–183.

Gay, N.C., 1966. Orientation of mineral lineation along the flow direction in rocks: a discussion. Tectonophysics 3, 559–564.

Gay, N.C., 1968a. The motion of rigid particles embedded in a viscous fluid during pure shear deformation of the fluid. Tectonophysics 5, 81–88.

Gay, N.C., 1968b. Pure shear and simple shear deformation of inhomogeneous viscous fluids. 1. Theory. Tectonophysics 5, 211–234.

Ghosh, S.K., Ramberg, H., 1976. Reorientation of inclusions by combination of pure shear and simple shear. Tectonophysics 34, 1–70.

Gierszewski, P.L., Chaffey, L.E., 1978. Rotations of an isolated triaxial ellipsoid suspended in slow viscous flow. Canadian Journal of Physics 56, 6–11.

Giorgis, S., Tikoff, B., 2004. Constraints on kinematics and strain from feldspar porphyroclast populations. In: Alsop, G., Holdsworth, R.E., McCaffrey, K.J.W., Hand, M. (Eds.), Flow Processes in Faults and Shear Zones. Geological Society, London, Special Publications, vol. 224, pp. 265–285.

Goldsmith, H.L., Mason, S.G., 1967. The microrheology of dispersions. In: Eirich, F.R. (Ed.), Rheology: Theory and Applications, vol. 4, pp. 85–250.

Harvey, P.K., Ferguson, C.C., 1978. A computer simulation approach to textural interpretation in crystalline rocks. In: Merriam, D.F. (Ed.), Recent Advances in Geomathematics. Pergamon, Oxford, pp. 201–232.

Hinch, E.J., Leal, L.G., 1979. Rotation of small non-axisymmetric particles in a simple shear flow. Journal of Fluid Mechanics 92, 591–608.

Hobbs, B.E., Means, W.D., Williams, P.F., 1976. An Outline of Structural Geology. John Wiley & Sons, New York.

Ildefonse, B., Launeau, P., Bouchez, J.L., Fernandez, A., 1992a. Effect of mechanical interactions on the development of shape preferred orientations: a two dimensional experimental approach. Journal of Structural Geology 14, 73–83.

Ildefonse, B., Mancktelow, N.S., 1993. Deformation around rigid particle: influence of slip at the particle/matrix interface. Tectonophysics 221, 345–359.

Ildefonse, B., Sokoutis, D., Mancktelow, N.S., 1992b. Mechanical interactions between rigid particles in a deforming ductile matrix. Analogue experiments in simple shear flow. Journal of Structural Geology 14, 1253–1266.

Jeffery, G.B., 1922. The motion of ellipsoidal particles immersed in a viscous fluid. Proceedings of the Royal Society of London A 102, 161–179.

Jeffrey, A., 1995. Handbook of Mathematical Formulas and Integrals. Academic Press, New York.

Ježek, J., 1994. Software for modeling the motion of rigid triaxial ellipsoidal particles in viscous flow. Computers and Geosciences 20, 409–424.

Ježek, J., Melka, R., Schulmann, K., Venera, Z., 1994. The behaviour of rigid ellipsoidal particles in viscous flows – modeling of fabric evolution in a multiparticle system. Tectonophysics 29, 165–180.

Ježek, J., Schulmann, K., Segeth, K., 1996. Fabric evolution of rigid inclusions during mixed coaxial and simple shear flows. Tectonophysics 257, 203–221.

Jiang, D. Numerical modeling of the motion of deformable ellipsoidal objects in slow viscous flows. Journal of Structural Geology, in press.

Jiang, D., Williams, P.F., 2004. Reference frame, angular momentum, and porphyroblast rotation. Journal of structural Geology 26, 2211–2224.

Launeau, P., Robin, P.-Y.F., 2005. Determination of fabric and strain ellipsoids from measured sectional ellipses – implementation and applications. Journal of Structural Geology 27, 2223–2233.

Lin, S., Jiang, D., Williams, P.F., 1998. Transpression (or transtension) zones of triclinic symmetry: natural example and theoretical modeling. In: Holdsworth, R.E., Strachan, R., Dewey, J.F. (Eds.), Continental Transpressional and Transtensional Tectonics. Geological Society, London, Special Publications, vol. 135, pp. 41–57.

Lin, S., Jiang, D., 2001. Using along-strike variation in strain and kinematics to define the movement direction of curved transpressional shear zones: an example from northwestern Superior Province, Manitoba. Geology 29, 767–770.

Lisle, R.J., 1985. Geological Strain Analysis, a Manual for the R_f/ϕ Method. Pergamon Press, New York.

Mancktelow, N.S., Arbaret, L., Pennacchinoni, G., 2002. Experimental observations on the effect of interface slip on rotation and stabilisation of rigid particles in simple shear and a comparison with natural mylonites. Journal of Structural Geology 24, 567–585.

Mandal, N., Misra, S., Samanta, S.K., 2005a. Rotation of single rigid inclusions embedded in an anisotropic matrix: a theoretical study. Journal of Structural Geology 27, 731–743.

Mandal, N., Samanta, S.K., Bhattacharyya, G., Chakraborty, C., 2003. Deformation of ductile inclusions in a multiple inclusion system in pure shear. Journal of Structural Geology 25, 1359–1370.

Mandal, N., Samanta, S.K., Bhattacharyya, G., Chakraborty, C., 2005b. Rotation behaviour of rigid inclusions in multiple association: insights from experimental and theoretical models. Journal of Structural Geology 27, 679–692.

Marques, F.O., Coelho, S., 2001. Rotation of rigid elliptical cylinders in viscous simple shear flow: analogue experiments. Journal of Structural Geology 23, 609–617.

Marques, F.O., Bose, S., 2004. Influence of a permanent low-friction boundary on rotation and flow in rigid inclusion/viscous matrix systems from an analogue perspective. Tectonophysics 382, 229–245.

Passchier, C.W., 1987. Stable positions of rigid inclusions in non-coaxial flow: a study in vorticity analysis. Journal of Structural Geology 9, 679–690.

Ramsay, J.G., 1967. Folding and Fracturing of Rocks. McGraw-Hill, New York.

Reed, L.J., Tryggvason, E., 1974. Preferred orientations of rigid particles in a viscous matrix deformed by pure shear and simple shear. Tectonophysics 24, 85–98.

Robin, P.-Y.F., 1977. Determination of geologic strain using randomly oriented strain markers of any shape. Tectonophysics 42, T7–T16.

Robin, P.-Y.F., 2002. Determination of fabric and strain ellipsoids from measured sectional ellipses – theory. Journal of Structural Geology 24, 531–544.

Sanderson, D.J., Meneilly, A.W., 1981. Analysis of three-dimensional strain modified uniform distributions: andalusite fabrics from a granite aureole. Journal of Structural Geology 3, 109–116.

Schmid, D.W., Podladchikov, Y.Y., 2004. Are isolated stable rigid clasts in shear zones equivalent to voids? Tectonophysics 384, 233–242.

Schmid, D.W., Podladchikov, Y.Y., 2005. Mantled porphyroclast gauges. Journal of Structural Geology 27, 571–585.

Taylor, G.I., 1923. The motion of ellipsoidal particles in a viscous fluid. Proceedings of the Royal Society of London A 103, 58–61.

Trevelyan, B.J., Mason, S.G., 1951. Particle motions in sheared suspensions. I. Rotations. Journal of Colloid Science 6, 354–367.

Tullis, T.E., 1976. Experiments on the origin of slaty cleavage and schistosity. Geological Society of America Bulletin 87, 745–753.

Willis, D.G., 1977. A kinematic model of preferred orientation. Geological Society of America Bulletin 88, 883–894.